nature neuroscience

Bi-stable neural state switches

André Berndt[1,5], Ofer Yizhar[2,5], Lisa A Gunaydin[2,3,5], Peter Hegemann[1] & Karl Deisseroth[2,4]

Here we describe bi-stable channelrhodopsins that convert a brief pulse of light into a stable step in membrane potential. These molecularly engineered probes nevertheless retain millisecond-scale temporal precision. Photocurrents can be precisely initiated and terminated with different colors of light, but operate at vastly longer time scales than conventional channelrhodopsins as a result of modification at the C128 position that extends the lifetime of the open state. Because of their enhanced kinetic stability, these step-function tools are also effectively responsive to light at orders of magnitude lower intensity than wild-type channelrhodopsins. These molecules therefore offer important new capabilities for a broad range of *in vivo* applications.

Three functionally distinct classes of microbial opsin genes, including channelrhodopsin and halorhodopsin family members, can transduce light pulse trains into millisecond time-scale membrane potential changes when expressed in neurons[1–3]. This property opens the door to optical control of specific cell types in the intact mammalian brain[4–9] and other systems[10–26], as a result of the essential feature shared by these microbial opsin genes of encoding single-component light-activated transmembrane ion conductance regulators[27–29]. The temporal properties of channelrhodopsins arise from inherently fast kinetics of activation and deactivation[2,3,28,30], allowing generation of precisely timed action-potential trains. However, at the levels of expression that are typically achieved in neurons, >1 mW mm^{-2} intensity light pulses must be generated and applied to tissue over the time period in which depolarization is required, which can pose challenges regarding power consumption and energy deposition for long time-scale experiments.

Alternatively, chemical photoswitches and caged compounds that act on ion channels permit stable changes in membrane current after brief flashes of light[31–33] and can support robust ionic currents. These approaches however are restricted by the requirement for delivery of extrinsic chemical cofactors and ultraviolet light, limiting *in vivo* applicability, with particular severity in mammals. Therefore, there has been great interest in the generation of a hypothetical bi-stable channelrhodopsin that would be gated into the active state with a single brief pulse of light and would remain active for a duration that is far longer than the light pulse, effectively processing the delta function of light into a step function of membrane potential. The advantages of such a technology would be enormous for many long–time scale, neuromodulatory, developmental and preclinical/clinical applications, and, if derived from channelrhodopsins, would maintain the important property of chemical cofactor independence in mammalian brains. However, it has been unclear how such a fundamental new property could be achieved with channelrhodopsins and how the resulting stable depolarization could be precisely terminated as needed at a specified time, particularly if the offset of depolarization is no longer coupled to the offset of the triggering light pulse itself.

We sought to address this challenge using directed molecular engineering of channelrhodopsin-2 (ChR2) to modify protein residues that are likely to be critical for determining the channel kinetics. Clues about the relevant residues arise from sequence comparisons with the well-characterized prokaryotic proton pump bacteriorhodopsin, for which the tertiary structure is available at high resolution[34,35]. Mutations introduced at key residues of bacteriorhodopsin lead to slowing of channel kinetics and accumulation of the M, N and O photocycle states[36,37]. On the basis of functional and structural inferences between bacteriorhodopsin and ChR2, we designed targeted mutations in the ChR2 sequence that would modify key steps in the photocycle of channelrhodopsin, such that the closing of the channel would be substantially delayed after optical activation. These mutations could modify the kinetic properties of ChR2-evoked currents and yield step-like, reversible changes in neuronal excitability.

RESULTS

Of the seven putative transmembrane helices in microbial rhodopsins, helix 3 contains the most amino acids that interact with the all-*trans* retinal Schiff base (RSB) chromophore. Many of these amino acids are conserved in channelrhodopsins (**Fig. 1a**), suggesting that color tuning[38] and the RSB switch that governs interconversion of nonconducting and conducting states is highly conserved[39]. Therefore, mutations of amino acids that interfere with the RSB are potential candidates, not only for color tuning, but also for altering kinetics and accumulation of the conducting state. Among the amino acids that interact with the RSB, the most notable sequence difference between bacteriorhodopsin and ChR2 was the Cys128 residue of ChR2, corresponding to Thr90 in bacteriorhodopsin (**Fig. 1a**). High-resolution X-ray crystallography and NMR studies have shown that Thr90 in bacteriorhodopsin is located close to the C11/C12 carbons of the protonated RSB[34,40,41] (**Fig. 1b**). Mutation of Thr90 to Ala or Val in bacteriorhodopsin results in a slowing of the photocycle kinetics and accumulation of the M, N and O photocycle states[36,42]. We reasoned that mutating C128 could potentially create a channelrhodopsin with delayed channel inactivation.

[1]Institute of Biology, Experimental Biophysics, Humboldt-University, Invalidenstraße 42, D-10115 Berlin, Germany. [2]Department of Bioengineering, [3]Neuroscience Program, [4]Department of Psychiatry and Behavioral Sciences, W083 Clark Center, 318 Campus Drive West, Stanford University, Stanford, California 94305, USA. [5]These authors contributed equally to this work. Correspondence should be addressed to P.H. (hegemape@rz.hu-berlin.de) or K.D. (deissero@stanford.edu).

Received 3 October; accepted 2 December; published online 8 December 2008; doi:10.1038/nn.2247

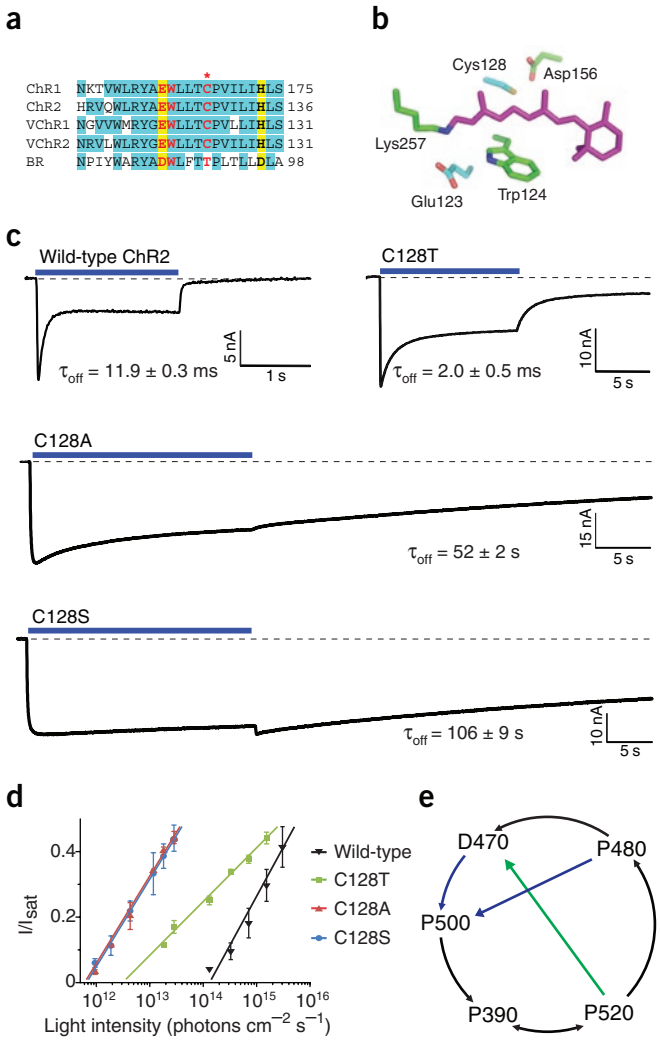

Figure 1 Step-function optogenetics: C128 mutations. (**a**) Alignment of helix 3 for the four known channelrhodopsins and bacteriorhodopsin (BR) from *H. salinarum*. Conserved residues are shown on a blue background, amino acids interacting with the chromophore are shown in red and the ChR2 C128 residue is marked with an asterisk. Amino acids that serve as H^+ donors or acceptors for RSB deprotonation and reprotonation are shown in yellow. (**b**) ChR2 chromophore model, based on the bacteriorhodopsin X-ray structure (1KGB[50]), with E123 and C128 of ChR2 replacing D85 and T90 of bacteriorhodopsin. (**c**) Photocurrents recorded from wild-type ChR2, C128T, C128A and C128S expressed in *Xenopus* oocytes at 100 mM NaCl (pH 7.5) and –50 mV in response to 450-nm light pulses (240 mW cm^{-2}, blue bars). Time constants shown are for the decay of current after termination of blue-light stimulation (mean ± s.e.m., $n = 5$ cells for each trace). (**d**) Light dependence of steady-state photocurrents recorded at low-light intensities. Cells that expressed C128A and C128S were ~300-fold more responsive to light than those that expressed wild-type ChR2. Amplitudes were normalized to the response at saturating light (I/I_{Sat}). (**e**) Model for the channelrhodopsin photocycle[43]. The D470 dark state with a protonated Schiff base is converted by a light-induced isomerization of retinal into the early intermediate P500. Transient deprotonation of the Schiff base (P390) leads to the conducting state P520. The recovery of the D470 dark state proceeds via the P480 intermediate, which is a nonconducting state, but can be excited by blue light (blue arrow) to yield the early intermediate P500. The closed D470 state can be accessed directly from P520 with green light (green arrow).

We expressed *ChR2-C128T*, *ChR2-C128A* and *ChR2-C128S* in *Xenopus* oocytes and recorded photocurrents in response to pulses of 470-nm blue light (**Fig. 1c**). Indeed, we found that the closing of the channel after light-off was slowed by three to four orders of magnitude in these mutants; we therefore designate these genes as step-function opsin (SFO) genes. Compared with the closing time constant (τ) of 11.9 ± 0.3 ms for wild-type ChR2 (at pH_o of 7.4 and –50 mV), we measured τ = 2.0 ± 0.5 s, 52 ± 2 s and 106 ± 9 s for the C128T, C128A and C128S mutants, respectively, revealing a marked extension of the lifetime of the conducting state (**Fig. 1c**). Because photocurrent amplitudes at a given light intensity are set by a balance between recruitment of new open states and transitions to the closed state, we expected that the increased accumulation of the open state would lead to an effectively increased responsiveness at lower light levels. Therefore, we tested the light-intensity dependence of stationary photocurrents; responses to light pulses of increasing intensity were recorded and normalized to the response at saturating light power (**Fig. 1d**). Notably, cells expressing the C128S and C128A mutants were responsive to light at an intensity that was at least 300-fold lower than those expressing wild-type ChR2, revealing a second important property of the SFO genes.

Although responsiveness to light was similar between C128S and C128A, C128S differed in two respects: C128S inactivated even more slowly than C128A and showed an additional small current peak on termination of the light pulse (**Fig. 1c**). Recent spectroscopic studies have shown that the P520 ChR2 photocycle intermediate reflects the channel open state absorbing maximally at 520 nm; that is, red-shifted relative to the dark state P470 (**Fig. 1e**)[43,44]. This photo-intermediate could undergo a photoreaction; brief flashes of green light applied during the open state prematurely closed the channel via conversion to the dark state D470 (**Fig. 1e**)[45]. The observed photocurrents revealed the accumulation of the conducting state P520, which is in equilibrium with the earlier nonconducting P390 state[43,44]. At light-off, P520 probably can no longer directly photoconvert to D470, and the resulting transient accumulation of conducting P520 state arising from P390 could give rise to the small peak that was observed at light-off in C128S (**Fig. 1e**). Consideration of this photocycle led us to develop a temporally precise method of terminating SFO currents.

Although the photo-intermediate P520 is normally so short-lived that the photochemical pathway to the nonconducting D470 state cannot be efficiently exploited, the extended lifetime of P520 in these C128 mutants presents the possibility of using green light to flip off the bi-stable switch. Indeed, we found that the inactivation dynamics of C128A and C128S were greatly accelerated when a second light pulse of longer wavelength followed the excitation pulse (**Fig. 2a**). The highest acceleration of the off-kinetics was seen with 530-nm light (which is close to the absorption maximum of the P520 conducting state), but the current inactivation was only partial, as a result of substantial absorption of this wavelength by the D470 dark state and potentially the late photo-intermediate P480 (**Fig. 2a**). In contrast, light of longer wavelength showed a slower, but more complete, inactivation, probably as a result of lower absorption by both D470 and P480, but improved absorption ratio (ε_{P520} to $\varepsilon_{P480/D470}$; **Fig. 1e**). We found pulses of 546-nm light to be optimal for suitably rapid and complete inactivation. Alternating 450-nm and 546-nm light allowed reversible ON and OFF switching without rundown (**Fig. 2b**), thereby defining a fast bi-stable switching mechanism for SFO genes.

This set of properties suggested that it would be important to test for prolonged, temporally precise activation of neurons. Some microbial opsin genes (for example, *ChR1*) are not expressed well in neurons;

however, we successfully expressed the three SFO genes (*ChR2-C128T*, *ChR2-C128A* and *ChR2-C128S*) as EYFP fusions in hippocampal neurons using lentiviral vectors that were driven by the *Camk2a* promoter[2]. All three mutants were well-tolerated in cultured neurons, with C128A and C128S appearing to be expressed at quantitatively reduced levels (**Fig. 3a**). We next recorded photocurrents evoked by 10-ms pulses of 470-nm light. Peak photocurrents recorded in C128T were similar to those of wild-type ChR2 (184 ± 34 and 240 ± 59 pA, respectively; $n = 10$ and 8 cells, respectively; **Fig. 3b**), whereas C128A and C128S both showed smaller photocurrent amplitudes (74 ± 17 and 61 ± 9 pA, respectively; $n = 11$ and 9 cells, respectively; **Fig. 3b**) and voltage changes (**Fig. 3c**). However, only brief flashes of up to 10 ms were needed for C128A/S to evoke near-maximal voltage changes (**Fig. 3d**) in all cases, suggesting that the photochemical equilibrium of dark state and conducting state is reached in a few milliseconds at a given light intensity. The apparent on-kinetics in all three mutants were only moderately slower than those of wild-type ChR2 (τ_{on} = 1.7 ± 0.1 ms, 11.6 ± 1.5 ms, 7.2 ± 0.8 ms and 20 ± 1.4 ms for ChR2, C128T, C128A and C128S, respectively; **Fig. 3e**,**f**). Notably, consistent with the oocyte data, mutant photocurrents decayed with up to four orders of magnitude slower kinetics (τ_{off} = 10 ± 0.8 ms, 1.8 ± 0.3 s, 49 ± 3.5 s and 108 ± 42 s, for wild-type ChR2, C128T, C128A and C128S, respectively; **Fig. 3g**,**h**), indicating that step-function properties were preserved in neurons.

We further explored the capacity of the mutant channels in neurons to elicit prolonged and reversible membrane depolarization in response to short light pulses. In neurons expressing C128S, one 10-ms flash of blue light (470 nm) was able to evoke markedly prolonged subthreshold depolarization (**Fig. 4a**) and chronic stimulation protocols consisting of just one 10-ms light pulse every 15 s enabled sustained stable depolarization over minutes that could be rapidly terminated with a single pulse of 535-nm light (**Fig. 4a**). Indeed, multiple precise steps could be reliably delivered and terminated in the same neurons using pairs of blue and green stimuli (**Fig. 4b**). Optimal inactivation after a 10-ms, 470-nm activation pulse was found to occur with slightly longer 50-ms pulses of 535-nm light (**Fig. 4b**,**c**), consistent with the fact that nearly all P520 molecules must be converted to P470 for a complete off response, whereas incomplete conversion of D470 to P520 is sufficient for an on response. Together, these data demonstrate bi-stable switching behavior in neurons.

The stable subthreshold depolarizations evoked by photostimulation of C128A- or C128S-expressing neurons may be most useful not for driving precisely timed spike trains (as with wild-type ChR2), but for generating modulated states of altered excitability (for example, subthreshold 5–10-mV step-like depolarizations that can modulate information throughput). Effectively sensitizing genetically targeted neurons to native, endogenous synaptic inputs will, in most cases, be the most suitable way to test the causal importance of a neuron type, as neuroscientists typically do not know the neural spike code for a particular cell type in executing its function, but could test the causal sufficiency of the cell type by expressing an SFO gene to stably and reversibly enhance natural patterns of information flow through those cells. To illustrate this principle with the SFO approach, we collected native excitatory postsynaptic potential (EPSP) trains with current-clamp recordings in nontransduced hippocampal pyramidal neurons, replayed the EPSP trains into C128A- or C128S-expressing cells before, during and after the 20 s-duration excitable states elicited by a single blue-light pulse (10 ms, 470 nm) and terminated with a single green-light pulse (50 ms, 535 nm; **Fig. 4d**). Before or after these states, EPSP trains produced little spiking (3.0 ± 1.1 spikes over 20 s), whereas the same EPSP train elicited greatly increased spiking in the excitable states (17 ± 3.5 spikes during the 20-s period, 9 out of 9 cells increased spiking;

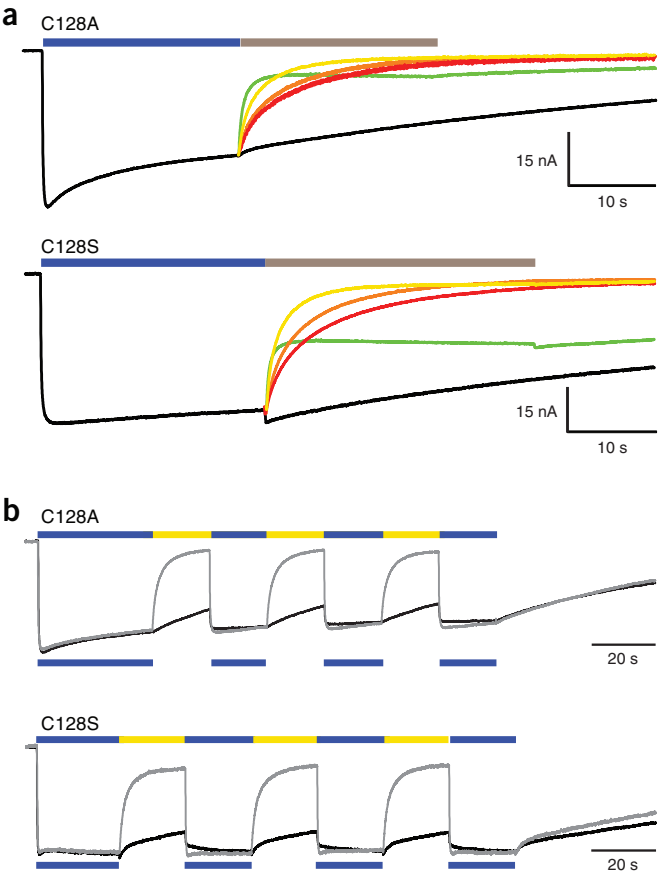

Figure 2 Precise step termination with red-shifted light. (**a**) Photocurrents recorded from C128A and C128S mutants. Off kinetics were accelerated when a second light pulse with longer wavelength (gray bar) followed the excitation pulse (green, 530 nm; yellow, 546 nm; orange, 570 nm; red, 600 nm). (**b**) Responses to alternating 450-nm and 546-nm light pulses (gray traces) or 450-nm light pulses only (black traces) in oocytes expressing C128A and C128S. Normalized currents are shown; colored bars on top and bottom indicate light-stimulation protocols for alternating blue/yellow and blue-only traces, respectively.

$P = 0.0006$, paired t test). Therefore, the SFO genes can be used for photostimulation that sensitizes neurons to ongoing synaptic activity on long time scales that can be precisely defined by the experimenter.

DISCUSSION

The engineered channelrhodopsins described here have fundamentally useful properties that allow the optical control of neurons over long time scales in a temporally precise manner and therefore (along with ChR2, VChR1 and NpHR) represent a fourth, functionally distinct class of microbial opsin–based tools. Different SFO genes may be useful for different experimental applications. Because it has faster activation kinetics and superior inactivation by green light, the C128A mutant may be best suited for experiments in which rapid activation and inactivation of photocurrents are required. The C128S mutant, which has even slower τ_{off} kinetics than C128A, would be ideal for experiments in which chronic excitation is required with minimal light delivery. Although the off kinetics of the C128T mutant are not nearly as slow as those of C128A/S, this mutant still offers a major improvement over ChR2 for applications in which driving spiking over a long period of time is desired; because of its robust expression levels, C128T currents

are already comparable to wild-type currents without additional engineering and therefore could induce temporally controlled bursts of action potentials in specific subpopulations of neurons. Compared with other optical tools for long-term excitation, these channels do not require infusion of chemical cofactors or ultraviolet-spectrum light.

The notable off kinetics and responsivity properties of these new channelrhodopsins can be understood in terms of cyclical models of the underlying photochemical reactions (**Fig. 1e**). After light excitation of the dark state D470, the conducting state P520 is reached via two early photochemical intermediates, P500 and P390. P520 is in a pH-dependent equilibrium with the deprotonated P390 (refs. 43,44) and decays in wild-type ChR2 with a time constant of ~10 ms[43,45]. The P520 to P480 conversion involves RSB reisomerization, probably from *13-cis* to *trans*, as with N-state decay of bacteriorhodopsin[37]. Close interaction of the polarizable Cys128 sulfur with the retinal polyene system could accelerate photo-isomerization, protonation, reisomerization and conformational changes in channelrhodopsins (**Fig. 1b**), beyond the maximal kinetics of all other microbial retinal proteins with Thr or Ser instead at this position. Conversely, mutation of C128 could delay formation of the conducting state and markedly slow reisomerization. The P520 decay in C128S was so slow that the late photocycle intermediate P480 (**Fig. 1e**) did not accumulate, with the consequence that the photocurrent was virtually not inactivated, even in continuous light (little desensitization will be a useful property with these more-responsive mutants). From studies of the homologous T90 in bacteriorhodopsin[46,47], the interaction of C128 with its presumptive counterion D156 (**Fig. 1b**) could plausibly have been critical, but the fact that the Ser and Ala C128 mutant kinetics are notably similar to each other indicates instead that the sulfur directly influences the retinylidene moiety.

The long open-time, but temporally precise, properties of these engineered microbial proteins would be well-suited for studying the role of specific cell types in neuroplasticity during development, as well as in homeostatic and adaptive processes in the adult brain or in chronic disease models. Furthermore, the SFO genes would be ideal for mimicking steps or oscillations in which a population of neurons alternates between a hyperpolarized and a depolarized (UP) state. UP states have been observed in cortex with an average depolarization of 11–12 mV (for example, see ref. 48) and are thought to be involved in systems-level phenomena such as attention and sensorimotor gating. Notably, UP states may or may not correspond to increased excitability, pointing to the need for informative experiments on modulation of circuit function that would directly test the sufficiency of step changes in membrane potential in defined cell types. Similarly, synchronous oscillations in membrane potential with an average amplitude of 7–8 mV lasting 1–2 s have been observed in nucleus accumbens medium spiny neurons[49] and are thought to be relevant to reward-related behavior. Thus, the amplitudes and temporal characteristics of both cortical and subcortical UP states are in the range of SFO-mediated currents.

In general, sensitizing targeted neurons to native synaptic drive in this way will demonstrate causal significance in a way that is complementary to ChR2-based synchronous driving of the entire targeted cell population, as action potential codes are typically not known by the experimenter, nor are cells of a particular type always naturally driven in synchrony. Precisely timed and reversible optogenetic modulation of excitability in defined cell types *in vivo,* by promoting throughput of asynchronous and distributed endogenous codes, will be crucial for defining the physiological causal importance of the targeted cells. It should be noted that calibration of the electrophysiological effects of SFO activation at a given expression level in cell types of interest will be important before application in behavioral experiments, because the net effect of step depolarization, as with any UP state, will depend on synaptic drive and the membrane-channel biophysical properties governing excitability, input resistance and refractory states.

In addition to allowing new basic science applications, reduced light requirements will have an enormous effect on optical hardware requirements in preclinical/clinical experiments, reducing power draw, heating and risks for long-term phototoxicity. Although the SFO genes already

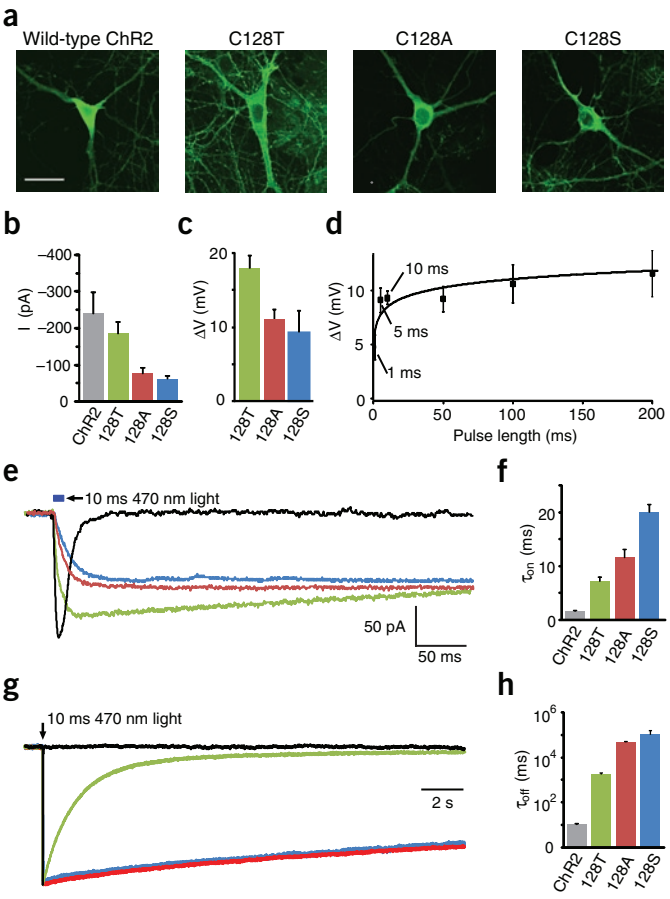

Figure 3 SFO genes in neurons. (**a**) Confocal images of cultured hippocampal neurons expressing wild-type ChR2, C128S, C128A and C128T under the *Camk2a* promoter. Intensity scaling and pixel size are identical in all images. Scale bar represents 25 µm. (**b**) Summary of photocurrents recorded from neurons expressing wild-type ChR2 and mutants, shown as mean ± s.e.m. (n = 8, 11, 9 and 10 for wild type, C128S, C128A and C128T, respectively). Cells were stimulated with a single 10-ms pulse of 470-nm blue light. (**c**) Depolarization induced by ChR2 mutants. Voltage recordings were made in neurons expressing C128S, C128A and C128T using the same stimulation protocol as in **b**. Peak depolarizations were averaged from 3, 7 and 7 cells for C128S, C128A and C128T mutants, respectively. (**d**) Summary of depolarization in C128A and C128S mutants in response to 470-nm light pulses of varying lengths (data are averaged from at least three cells for each pulse length). (**e**) Expanded view of photocurrents evoked by a 10-ms pulse of 470-nm blue light in neurons expressing wild-type ChR2 (gray), C128S (blue), C128A (red) and C128T (green) showing slower on kinetics for the mutants. (**f**) Summary of on kinetics in response to 10-ms blue-light stimulation. Shown are mean time constants from exponential fits to current traces; although onset kinetics of C128S and C128A are similar in the traces in **e**, C128S was typically slower than C128A, as summarized here. (**g**) Slower decay time constants of photocurrents in the C128 mutants. Traces are normalized to the peak photocurrent in each mutant. (**h**) Summary of off kinetics in C128 mutants. Mean time constants were derived from exponential fits.

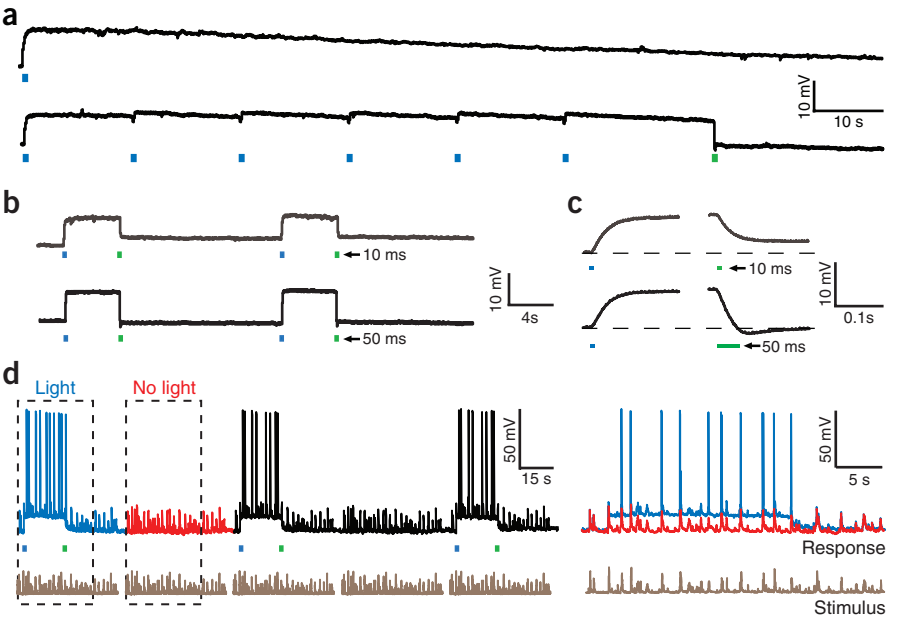

Figure 4 Bi-stable switching behavior in neurons. (**a**) Whole-cell current-clamp recording from a cultured rat hippocampal neuron expressing C128S under the *Camk2a* promoter. Subthreshold depolarization was induced by a single 10-ms pulse of 470-nm light (blue dash indicates time of stimulus, top) or by several widely spaced 10-ms pulses of 470-nm light (each pulse indicated by a blue dash, bottom). Because of the long time base, light pulse dashes are not to scale in this figure. (**b**) Whole-cell current-clamp recording from a hippocampal neuron expressing C128S stimulated with pairs of 470-nm and 535-nm light pulses. Top, the response to a 10-ms pulse of blue light followed by a 10-ms pulse of green light is shown. Bottom, the response to a 10-ms pulse of blue light followed by a 50-ms pulse of green light (indicated by blue and green dashes, respectively) is shown. Stimulus pairs were given at 20-s intervals and the interval in each stimulus pair was 5 s. (**c**) Magnified traces from the bottom stimulus pair in **b** show complete inactivation with 50 ms of green light. The resting membrane potential is indicated by the broken line. (**d**) Left, whole-cell current-clamp recording from a hippocampal neuron expressing C128A stimulated with a pre-recorded EPSP trace. The recorded EPSP trace was delivered in five identical blocks (brown lines). During blocks 1, 3 and 5, pairs of 470-nm and 535-nm light stimuli (10 ms and 50 ms, respectively; indicated by blue and green dashes) were delivered to induce subthreshold depolarization. During blocks 2 and 4, no light was delivered. Right, expanded view of response to EPSPs with and without light (blue and red traces, respectively; overlay of dashed black boxes) shows the light-induced increase in spiking to EPSP stimuli (brown trace).

are suitable for experiments in which step changes in excitability are required (**Fig. 4**), photocurrents are very likely to be enhanced with further engineering (for example, double mutation of C128 and H134 (ref. 8,19), red-shifted VChR1 versions for recruiting larger volumes of tissue with lower-energy photons[3] and molecular modifications to increase membrane trafficking, as with eNpHR[7,26]). Their stability and light responsivity, coupled with precise on and off switching and the chemical cofactor independence of channelrhodopsins, offer a constellation of key characteristics for use in both basic and applied research into intact neural circuitry.

METHODS

All experiments were conducted under protocols approved by the Stanford Administrative Panel on Laboratory Animal Care.

Sequence alignment and homology model of bacteriorhodopsin. Sequences were aligned by using the NCBI/BLAST-program (http://blast.ncbi.nlm.nih.gov/) with some final manual editing. The accession numbers for sequences shown in **Figure 1a** are AF385748(ChR1), AF461397(ChR2), EU285659(VChR1) and EU285660(VChR2). The chromophore model in **Figure 1b** is based on the dark state structure of bacteriorhodopsin (1KGB)[50]. Replacement of amino acid residues was carried out using MacPyMOL (DeLano Scientific LLC; http://www.csb.yale.edu/).

Expression and electrophysiology of ChR2 mutants in *Xenopus laevis* oocytes. For oocyte experiments, we introduced mutations into the pGEMHE-ChR2 plasmid using site-directed mutagenesis. cRNAs encoding ChR2(1–315) (ref. 28), C128A, C128S and C128T, synthesized *in vitro* from the pGEMHE plasmid by T7 RNA polymerase (mMessage mMachine, Ambion), were injected into the oocytes (50 ng per cell). The oocytes were stored for 3–7 d in the dark at 18 °C in Ringer solution (96 mM NaCl, 5 mM KCl, 1.8 mM CaCl2, 1 mM MgCl2 and 5 mM MOPS-NaOH, pH 7.5) in the presence of 1 mg ml^{-1} penicillin, 1 mg ml^{-1} streptomycin, 1 μM all-trans retinal (stock, 1 mM in 2-propanol) and 0.5 mM theophylline. Two-electrode voltage-clamp measurements on *Xenopus laevis* oocytes were performed with a Turbo Tec-05X (NPI Electronic). Data acquisition and light triggering were controlled with pCLAMP software via DigiData 1322A or 1440A interfaces (Molecular Devices). The microelectrodes were fabricated by pulling borosilicate glass capillaries (1.5-mm outer diameter and 1.17-mm inner diameter) using a micropipette puller (model P-97, Sutter Instruments) and filled with 3 M KCl. A 75-W Xenon lamp (Jena Instruments) was used as light source. The light was passed through either a K450 filter (50-nm half band width, Balzers) or narrow-band interference filters (14–20 nm half band width, AHF) and applied to the oocytes by a light guide (2-mm diameter). The light intensity is given in the legends for the surface of the oocyte. The data obtained were averages of more than three experiments. Data acquisition and light triggering were controlled with pCLAMP software via DigiData 1440A interfaces (Molecular Devices). Data were recorded with a sampling rate of 1–10 kHz in external solution containing 100 mM NaCl, 1 mM MgCl2 and 0.1 mM CaCl2, buffered with 5 mM MOPS.

Hippocampal neuron culture. Hippocampi were isolated from postnatal day 0 (P0) Sprague-Dawley rats (Charles River) and treated with papain (20 U ml^{-1}) for 45 min at 37 °C. The digestion was stopped with 10 ml of MEM/Earle's salts without L-glutamine along with 20 mM glucose, Serum Extender (1:1,000) and 10% heat-inactivated fetal bovine serum containing 25 mg of bovine serum albumin and 25 mg of trypsin inhibitor. The tissue was triturated in a small volume of this solution with a fire-polished Pasteur pipette and ~100,000 cells in 1 ml were plated per cover slip in 24-well plates. Glass coverslips (prewashed overnight in HCl followed by several 100% ethanol washes and flame sterilization) were coated overnight at 37 °C with 1:50 Matrigel (Collaborative Biomedical Products). Cells were plated in culture medium (Neurobasal containing 2× B-27 and 2 mM Glutamax-I, Life Technologies). We replaced half of the medium with culture medium the next day, giving a final serum concentration of 1.75%. No all-trans retinal was added to the culture medium or recording medium for any of the neuronal experiments described here.

Hippocampal neuron electrophysiology. For whole-cell recording in cultured hippocampal neurons, the intracellular solution contained 129 mM potassium gluconate, 10 mM HEPES, 10 mM KCl, 4 mM Mg-ATP and 0.3 mM Na-GTP, titrated to pH 7.2. Tyrode's solution was employed as the extracellular solution (125 mM NaCl,

2 mM KCl, 2 mM $CaCl_2$, 1 mM $MgCl_2$, 30 mM glucose and 25 mM HEPES, titrated to pH 7.4). Recordings were conducted on an upright Leica DM-LFSA microscope equipped with a 40× water-immersion objective. Borosilicate glass (Sutter Instruments) pipette resistances were ~5 MΩ, with a range of 4–6 MΩ. Access resistance was 10–35 MΩ and was monitored for stability throughout the recording. All recordings were conducted in the presence of excitatory synaptic transmission blockers (10 μM 6-cyano-7-nitroquinoxaline-2,3-dione and 25 μM D(–)-2-amino-5-phosphonovaleric acid, Sigma). For hippocampal neuron photostimulation, the filters used in the Lambda DG-4 optical switch (Sutter Instruments) with a 300-W Xenon lamp were 470 (HQ470/40), and 535 nm (HQ535/50) (Chroma).

Lentiviral vector construction. *ChR2-C128A*, *ChR2-C128S* and *ChR2-C128T* were constructed by site-directed mutagenesis (Quikchange, Invitrogen) to the pLenti-CaMKIIa-ChR2-EYFP-WPRE vector described previously[1]. Briefly, PCR reactions were carried out using the above plasmid as template. High-performance liquid chromatography–purified primers (Operon Technologies) were used to introduce the mutated bases. The primer sequences for *ChR2-C128A*, *ChR2-C128S* and *ChR2-C128T* were 5′-CTA TGC AGA GTG GCT GCT CAC TGC CCC TGT CAT CCT TAT C-3′, 5′-CTA TGC AGA GTG GCT GCT CAC TTC TCC TGT CAT CCT TAT C-3′, 5′-CTA TGC AGA GTG GCT GCT CAC TAC TCC TGT CAT CCT TAT C-3′, respectively. All mutations were then confirmed by DNA sequencing. VSVg-pseudotyped recombinant lentiviruses were produced as described previously[1] (detailed at http://www.stanford.edu/group/dlab/optogenetics/expression_systems) by triple-transfection of HEK 293FT cells (Invitrogen) with pLenti-CaMKIIa-ChR2-EYFP-WPRE or the mutated plasmids, pVSVg and pCMVdeltaR8.7. Virus supernatant was collected 40 h after transfection and applied to neurons.

ACKNOWLEDGMENTS

A.B. is supported by a Leibniz Graduate School fellowship, O.Y. by an European Molecular Biology Organization long-term postdoctoral fellowship and L.A.G. by a Stanford Bio-X Graduate Fellowship. P.H. is supported by the Deutsche Forschungsgemeinschaft (SFB498 and CoE: Unifying concepts in Catalysis). K.D. is supported by the California Institute of Regenerative Medicine, the McKnight and Wallace H. Coulter Foundations, the National Science Foundation, the US National Institute of Mental Health, the US National Institute on Drug Abuse, the US National Institutes of Health Pioneer Award, and the Kinetics and Keck Foundations.

Published online at http://www.nature.com/natureneuroscience/
Reprints and permissions information is available online at http://www.nature.com/reprintsandpermissions/

1. Zhang, F. *et al.* Multimodal fast optical interrogation of neural circuitry. *Nature* **446**, 633–639 (2007).
2. Boyden, E.S., Zhang, F., Bamberg, E., Nagel, G. & Deisseroth, K. Millisecond-timescale, genetically targeted optical control of neural activity. *Nat. Neurosci.* **8**, 1263–1268 (2005).
3. Zhang, F. *et al.* Red-shifted optogenetic excitation: a tool for fast neural control derived from *Volvox carteri*. *Nat. Neurosci.* **11**, 631–633 (2008).
4. Adamantidis, A.R., Zhang, F., Aravanis, A.M., Deisseroth, K. & de Lecea, L. Neural substrates of awakening probed with optogenetic control of hypocretin neurons. *Nature* **450**, 420–424 (2007).
5. Aravanis, A.M. *et al.* An optical neural interface: in vivo control of rodent motor cortex with integrated fiberoptic and optogenetic technology. *J. Neural Eng.* **4**, S143–S156 (2007).
6. Arenkiel, B.R. *et al.* In vivo light-induced activation of neural circuitry in transgenic mice expressing channelrhodopsin-2. *Neuron* **54**, 205–218 (2007).
7. Gradinaru, V., Thompson, K.R. & Deisseroth, K. eNpHR: a *Natronomonas* halorhodopsin enhanced for optogenetic applications. *Brain Cell Biol.* **36**, 129–139 (2008).
8. Gradinaru, V. *et al.* Targeting and readout strategies for fast optical neural control *in vitro* and *in vivo*. *J. Neurosci.* **27**, 14231–14238 (2007).
9. Huber, D. *et al.* Sparse optical microstimulation in barrel cortex drives learned behavior in freely moving mice. *Nature* **451**, 61–64 (2008).
10. Bi, A. *et al.* Ectopic expression of a microbial-type rhodopsin restores visual responses in mice with photoreceptor degeneration. *Neuron* **50**, 23–33 (2006).
11. Campagnola, L., Wang, H. & Zylka, M.J. Fiber-coupled light-emitting diode for localized photostimulation of neurons expressing channelrhodopsin-2. *J. Neurosci. Methods* **169**, 27–33 (2008).
12. Douglass, A.D., Kraves, S., Deisseroth, K., Schier, A.F. & Engert, F. Escape behavior elicited by single, channelrhodopsin-2–evoked spikes in zebrafish somatosensory neurons. *Curr. Biol.* **18**, 1133–1137 (2008).
13. Farah, N., Reutsky, I. & Shoham, S. Patterned optical activation of retinal ganglion cells. *Conf. Proc. IEEE Eng. Med. Biol. Soc., 2007* 6369–6371 (2007).
14. Han, X. & Boyden, E.S. Multiple-color optical activation, silencing, and desynchronization of neural activity, with single-spike temporal resolution. *PLoS ONE* **2**, e299 (2007).
15. Hwang, R.Y. *et al.* Nociceptive neurons protect *Drosophila* larvae from parasitoid wasps. *Curr. Biol.* **17**, 2105–2116 (2007).
16. Ishizuka, T., Kakuda, M., Araki, R. & Yawo, H. Kinetic evaluation of photosensitivity in genetically engineered neurons expressing green algae light-gated channels. *Neurosci. Res.* **54**, 85–94 (2006).
17. Lagali, P.S. *et al.* Light-activated channels targeted to ON bipolar cells restore visual function in retinal degeneration. *Nat. Neurosci.* **11**, 667–675 (2008).
18. Li, X. *et al.* Fast noninvasive activation and inhibition of neural and network activity by vertebrate rhodopsin and green algae channelrhodopsin. *Proc. Natl. Acad. Sci. USA* **102**, 17816–17821 (2005).
19. Nagel, G. *et al.* Light activation of channelrhodopsin-2 in excitable cells of *Caenorhabditis elegans* triggers rapid behavioral responses. *Curr. Biol.* **15**, 2279–2284 (2005).
20. Petreanu, L., Huber, D., Sobczyk, A. & Svoboda, K. Channelrhodopsin-2–assisted circuit mapping of long-range callosal projections. *Nat. Neurosci.* **10**, 663–668 (2007).
21. Schroll, C. *et al.* Light-induced activation of distinct modulatory neurons triggers appetitive or aversive learning in *Drosophila* larvae. *Curr. Biol.* **16**, 1741–1747 (2006).
22. Toni, N. *et al.* Neurons born in the adult dentate gyrus form functional synapses with target cells. *Nat. Neurosci.* **11**, 901–907 (2008).
23. Wang, H. *et al.* High-speed mapping of synaptic connectivity using photostimulation in channelrhodopsin-2 transgenic mice. *Proc. Natl. Acad. Sci. USA* **104**, 8143–8148 (2007).
24. Zhang, F., Wang, L.P., Boyden, E.S. & Deisseroth, K. Channelrhodopsin-2 and optical control of excitable cells. *Nat. Methods* **3**, 785–792 (2006).
25. Zhang, Y.P. & Oertner, T.G. Optical induction of synaptic plasticity using a light-sensitive channel. *Nat. Methods* **4**, 139–141 (2007).
26. Zhao, S. *et al.* Improved expression of halorhodopsin for light-induced silencing of neuronal activity. *Brain Cell Biol.* **36**, 141–154 (2008).
27. Kalaidzidis, I.V., Kalaidzidis, Y.L. & Kaulen, A.D. Flash-induced voltage changes in halorhodopsin from *Natronobacterium pharaonis*. *FEBS Lett.* **427**, 59–63 (1998).
28. Nagel, G. *et al.* Channelrhodopsin-2, a directly light-gated cation-selective membrane channel. *Proc. Natl. Acad. Sci. USA* **100**, 13940–13945 (2003).
29. Oesterhelt, D., Hegemann, P. & Tittor, J. The photocycle of the chloride pump halorhodopsin. II. Quantum yields and a kinetic model. *EMBO J.* **4**, 2351–2356 (1985).
30. Hegemann, P., Ehlenbeck, S. & Gradmann, D. Multiple photocycles of channelrhodopsin. *Biophys. J.* **89**, 3911–3918 (2005).
31. Miesenböck, G. & Kevrekidis, I.G. Optical imaging and control of genetically designated neurons in functioning circuits. *Annu. Rev. Neurosci.* **28**, 533–563 (2005).
32. Szobota, S. *et al.* Remote control of neuronal activity with a light-gated glutamate receptor. *Neuron* **54**, 535–545 (2007).
33. Volgraf, M. *et al.* Allosteric control of an ionotropic glutamate receptor with an optical switch. *Nat. Chem. Biol.* **2**, 47–52 (2006).
34. Luecke, H., Schobert, B., Richter, H.T., Cartailler, J.P. & Lanyi, J.K. Structural changes in bacteriorhodopsin during ion transport at 2 angstrom resolution. *Science* **286**, 255–261 (1999).
35. Belrhali, H. *et al.* Protein, lipid and water organization in bacteriorhodopsin crystals: a molecular view of the purple membrane at 1.9-A resolution. *Structure* **7**, 909–917 (1999).
36. Peralvarez-Marin, A., Marquez, M., Bourdelande, J.L., Querol, E. & Padros, E. Thr-90 plays a vital role in the structure and function of bacteriorhodopsin. *J. Biol. Chem.* **279**, 16403–16409 (2004).
37. Schobert, B., Brown, L.S. & Lanyi, J.K. Crystallographic structures of the M and N intermediates of bacteriorhodopsin: assembly of a hydrogen-bonded chain of water molecules between Asp-96 and the retinal Schiff base. *J. Mol. Biol.* **330**, 553–570 (2003).
38. Wanko, M., Hoffmann, M., Frahmcke, J., Frauenheim, T. & Elstner, M. Effect of polarization on the opsin shift in rhodopsins. 2. Empirical polarization models for proteins. *J. Phys. Chem. B* **112**, 11468–11478 (2008).
39. Hegemann, P. Algal sensory photoreceptors. *Annu. Rev. Plant Biol.* **59**, 167–189 (2008).
40. Luecke, H., Schobert, B., Richter, H.T., Cartailler, J.P. & Lanyi, J.K. Structure of bacteriorhodopsin at 1.55 A resolution. *J. Mol. Biol.* **291**, 899–911 (1999).
41. Patzelt, H. *et al.* The structures of the active center in dark-adapted bacteriorhodopsin by solution-state NMR spectroscopy. *Proc. Natl. Acad. Sci. USA* **99**, 9765–9770 (2002).
42. Lanyi, J.K. & Schobert, B. Mechanism of proton transport in bacteriorhodopsin from crystallographic structures of the K, L, M1, M2 and M2' intermediates of the photocycle. *J. Mol. Biol.* **328**, 439–450 (2003).
43. Ritter, E., Stehfest, K., Berndt, A., Hegemann, P. & Bartl, F.J. Monitoring light induced structural changes of channelrhodopsin-2 by UV/Vis and fourier transform infrared spectroscopy. *J. Biol. Chem.* **283**, 35033–35041 (2008).
44. Ernst, O.P. *et al.* Photoactivation of channelrhodopsin. *J. Biol. Chem.* **283**, 1637–1643 (2008).
45. Bamann, C., Kirsch, T., Nagel, G. & Bamberg, E. Spectral characteristics of the photocycle of channelrhodopsin-2 and its implication for channel function. *J. Mol. Biol.* **375**, 686–694 (2008).
46. Flitsch, S.L. & Khorana, H.G. Structural studies on transmembrane proteins. 1. Model study using bacteriorhodopsin mutants containing single cysteine residues. *Biochemistry* **28**, 7800–7805 (1989).
47. Joh, N.H. *et al.* Modest stabilization by most hydrogen-bonded side-chain interactions in membrane proteins. *Nature* **453**, 1266–1270 (2008).
48. Sanchez-Vives, M.V. & McCormick, D.A. Cellular and network mechanisms of rhythmic recurrent activity in neocortex. *Nat. Neurosci.* **3**, 1027–1034 (2000).
49. Goto, Y. & O'Donnell, P. Network synchrony in the nucleus accumbens *in vivo*. *J. Neurosci.* **21**, 4498–4504 (2001).
50. Facciotti, M.T. *et al.* Structure of an early intermediate in the M-state phase of the bacteriorhodopsin photocycle. *Biophys. J.* **81**, 3442–3455 (2001).